Soft X-Ray Spectroscopy of Rare-Earth Elements in LHD Plasmas

Chihiro Suzuki [1],* , **Fumihiro Koike [2]** , **Izumi Murakami [1,3]** , **Naoki Tamura [1]** , **Shigeru Sudo [4]** **and Gerry O'Sullivan [5]**

1   Department of Helical Plasma Research, National Institute for Fusion Science, 322-6 Oroshi-cho, Toki 509-5292, Japan
2   Faculty of Science and Technology, Sophia University, 7-1 Kioi-cho, Chiyoda-ku, Tokyo 102-8554, Japan
3   Department of Fusion Science, SOKENDAI (The Graduate University for Advanced Studies), 322-6 Oroshi-cho, Toki 509-5292, Japan
4   College of Engineering, Chubu University, 1200 Matsumoto-cho, Kasugai 487-8501, Japan
5   School of Physics, University College Dublin, Belfield, Dublin 4, Ireland
*   Correspondence: csuzuki@nifs.ac.jp

Abstract: Soft X-ray spectra from high Z rare-earth (lanthanide) elements have been systematically observed in optically thin, high-temperature plasmas produced in the Large Helical Device (LHD), a facility for magnetically confined fusion research. It has been demonstrated that the discrete and quasicontinuum (UTA) spectral features from highly charged lanthanide ions are observed depending on the plasma temperature. The analyses of the measured spectra are ongoing by comparisons with theoretical calculations and/or previous experimental data available. The discrete spectra recorded in high-temperature conditions are dominated by individual lines of Ge- to Ni-like ions, while prominent peaks in the narrowed UTA spectra observed in low-temperature conditions are well explained by the transitions of Ag- to Rh-like ions.

1. Introduction

Soft X-ray emissions (roughly in the range of 1–10 nm) from high Z rare-earth elements (lanthanides) mainly originate from highly charged ions with $n = 4$ (N-shell) outermost electrons. Emission spectra of such rare-earth ions are of great interest in terms of atomic physics issues related to the properties of N-shell electrons: configuration mixing, orbital collapse, giant resonances, and so on [1–3]. In addition, some of the lanthanide elements are potentially important in plasma applications to short-wavelength light sources for the future semiconductor lithography in the wavelength range of 6–7 nm [4–9].

Soft X-ray spectra from high Z rare-earth elements have been experimentally studied so far using various light sources such as vacuum sparks [4,10], laser-produced plasmas (LPPs) [11–16], magnetically confined fusion (MCF) plasmas [17–25], and electron beam ion traps (EBITs) [26–29]. Systematic observations of the spectra for most lanthanide elements have been performed in earlier studies using high density LPPs under higher opacity conditions [13,14], in which quasicontinuum broadband spectral features with few isolated lines were typically observed as a result of higher opacity. More recently, soft X-ray spectra of LPPs of several lanthanide elements have been observed using an Nd:YAG laser and an X-ray charge coupled device (CCD) camera, which results in more detailed analyses of the quasicontinuum features and some individual lines [15,16]. Nevertheless, optically thin plasmas would be more suitable for exploring detailed structures of the measured spectra.

Soft X-ray spectroscopy in optically thin conditions have been extensively carried out in the Texas Experimental Tokamak (TEXT) for several lanthanide elements [17–22]. In these earlier studies, lanthanide elements have been injected into low-density ($\simeq 10^{19}$ m^{-3}) and high-temperature ($\simeq 1$ keV) plasmas using laser blow-off technique. As a result, broad features and some isolated lines are mixed up in the observed spectra. In EBIT facilities, charge-resolved soft X-ray spectra of some selected lanthanide elements have been recorded under extremely low-density conditions [26–29]. Nevertheless, experimental surveys of the spectra are still incomplete as there remains some lanthanide elements which have not been measured yet in these experiments.

In comparison with the earlier MCF devices, modern large-scale MCF devices realize better plasma performance: better stability, higher brightness, and higher temperature as high as several keV. Also, they are often equipped with powerful and novel diagnostic tools including pellet injection systems to introduce impurities directly into the plasma core region. In that sense, it would be meaningful to perform systematic studies on the spectra of rare-earth ions in modern MCF plasmas.

From this point of view, we have systematically observed soft X-ray spectra from highly charged lanthanide ions in plasmas produced in the Large Helical Device (LHD) at the National Institute for Fusion Science (NIFS) [23–25]. As a result, it has been demonstrated so far that the discrete and quasicontinuum spectral features from lanthanide ions with outermost N shell electrons are observed in high- and low-temperature conditions, respectively, and some isolated spectral lines from ions with simple electron configurations have been identified [23–25]. However, the detailed structures of the observed spectral features have not been fully analyzed yet. In this article, recent progress of the ongoing analysis using a variety of methods is presented together with a brief overview of the systematic observations.

2. Experimental

In this study, the LHD, a large-scale MCF device of helical type [30,31], is used to collect the spectral data for lanthanide elements in optically thin, high-temperature plasmas. The electron temperature and density in LHD plasmas are typically several keV and on the order of 10^{19} m^{-3}, respectively. The plasma volume is roughly 30 m^3, and the diameter of the entire structure of the torus is 13.5 m including superconducting coils generating a stable magnetic field of about 2.75 T. The LHD is equipped with powerful diagnostic tools for spectroscopic studies of high Z impurity ions injected into hydrogen/deuterium plasmas. Since this experimental setup has already been reported in the earlier papers [23–25], only a brief review is given here.

Lanthanide elements are introduced as impurities in LHD plasmas using tracer encapsulated solid pellet (TESPEL) [32,33], a tiny hollow plastic ball in which small amounts ($\simeq 10^{17}$ atoms) of powders or fragments of pure metals are encapsulated. Until now, all lanthanide elements except for lanthanum (La) and promethium (Pm) have already been injected in LHD plasmas [23–25]. The electron temperature and density profiles are measured by a Thomson scattering diagnostic with very high spatial and temporal resolutions [34,35].

Time evolutions of the soft X-ray spectra are recorded by a 2 m grazing incidence spectrometer [36] with a frame rate of 5–10 Hz. The 600 mm^{-1} groove density of the grating results in a wavelength resolution of approximately 0.01 nm. The wavelength coverage of the grating is approximately 3 nm, which is movable in the range of 1–35 nm. The plasma temperature rapidly drops due to a massive pellet injection or reduced heating power, which sometimes forms a 'temperature hole' [24,37,38]. In this way, we can acquire a variety of spectral data for a wide temperature range in a single discharge.

3. Temperature Dependent Spectral Feature

As mentioned in Section 1, major emitters in the soft X-ray region are ions with N-shell outermost electrons for lanthanide elements. The Z dependence of the soft X-ray spectra from N-shell lanthanide ions with atomic numbers of 60–70 has been systematically observed at different temperatures in the range of roughly 0.2–3 keV using the technique to scan the plasma temperature as mentioned in

Section 2. Since the details of the systematic observation has been reported in our previous paper [25], only a summary is shown here in this section.

The spectral features drastically change between quasicontinuum and discrete depending on the plasma temperature. The spectral features are almost discrete in high-temperature conditions as high as 1.5–2.4 keV. As the temperature decreases, the spectrum is dominated by a quasicontinuum feature, which is often called an unresolved transition array (UTA) [39], with a bandwidth of approximately 0.5 nm. When the temperature further decreases enough to form a temperature hole, the UTA bandwidth tends to be narrower ($\simeq$0.2 nm). This drastic change in the spectral feature can be explained by the change in ion abundance from higher to lower charge states within N shell ions. The discrete features in the high-temperature spectra originate from ions with 4s or 4p outermost electrons. Indeed, isolated lines due to $3d^{10}4p\ ^2P_{1/2}$–$3d^{10}4d\ ^2D_{3/2}$ transition of Cu-like ions (the highest charge state of N shell ions) are easily identified for nine elements. Some of these lines have been experimentally found for the first time in LHD. On the other hand, the broad UTA features in low-temperature conditions are composed of a huge number of lines arising from lower ion stages with 4d or 4f outermost electrons. Also, some of the isolated lines of Pd- or Ag-like ions have been identified in the narrowed UTA features observed in the lowest temperature cases.

The measured wavelengths of the four transition types of Cu-, Ag-, and Pd-like ions have been compared with the wavelengths calculated by GRASP92/RATIP codes [40,41]. The calculated wavelengths for $3d^{10}4p\ ^2P_{1/2}$–$3d^{10}4d\ ^2D_{3/2}$ transition of Cu-like ions are in very good agreement with the measurements, while the calculated wavelengths for $4d^{10}4f\ ^2F$–$4d^94f^2\ ^2G$ transition of Ag-like ions and $4d^{10}\ ^1S_0$–$4d^94f\ ^1P_1$ transition of Pd-like ions are systematically shifted to shorter wavelengths from the measurements.

In fact, the spectra measured in LHD plasmas are usually composed not only of simple ions (e.g., Cu-, Ag-, and Pd-like ions) but also of a wide range of ion stages. To further analyze such a complex spectrum, comparisons with theoretical models and/or other experimental data are indispensable. The further analysis is currently being performed by several different atomic codes and existing experimental data taken in different light sources. As for theoretical calculations, we employ non-relativistic or fully relativistic atomic codes such as Cowan [42], Hullac [43], FAC [44], and GRASP92/RATIP [40,41]. Collisional-radiative (CR) models are constructed based on the Hullac code because its calculation is fast and fully relativistic. Also, we compare with other experimental data taken in EBITs, tokamaks, and LPPs. Recent results of the ongoing analysis are described in Sections 4 and 5.

4. Analysis of High-Temperature Spectra

Discrete spectra observed in high-temperature conditions are easier to analyze because the number of lines is less and individual spectral lines are well isolated. Figure 1 shows soft X-ray spectra of thulium (Tm), erbium (Er), and samarium (Sm) ions recorded in LHD plasmas under high-temperature conditions. The peak electron temperatures are 2.4, 2.5 and 1.5 keV for Tm, Er, and Sm, respectively, as indicated in Figure 1.

Earlier experimental data available for Tm ions are very limited in particular for higher ion stages. Therefore, we compare the measured Tm spectrum with the results of a CR model constructed based on the Hullac code. In our model, a rate equation for each energy level of a particular ion stage is individually solved including electron impact excitation, de-excitation and ionization, and the spontaneous emission [38]. Recombination processes are ignored at this moment. As a result, the measured Tm spectrum is well reproduced by the model although the calculated wavelengths of some of the lines are slightly shifted to shorter wavelengths from the measurements. Consequently, seven prominent lines indicated by arrows in the top panel of Figure 1 have been successfully assigned for the first time in LHD as listed in Table 1. In earlier studies, the predicted wavelengths [45,46] have been reported only for the two lines presently observed at 6.072 and 7.753 nm, which are in good agreement with the predictions.
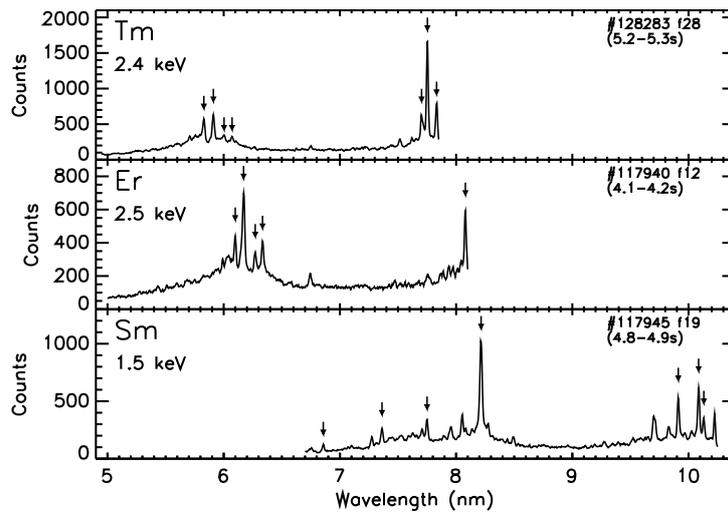
Figure 1. Soft X-ray spectra of thulium (top panel), erbium (middle panel), and samarium (bottom panel) ions recorded in LHD plasmas under high-temperature conditions. The peak electron temperature for each spectrum is shown in each panel. The assignments of the spectral lines indicated by arrows are summarized in Tables 1–3.

Table 1. The assignments of the lines of thulium ions indicated by arrows in the top panel of Figure 1. The assignments are based on a CR model constructed based on the Hullac code. Isoelectronic sequence of each ion is shown in a square bracket. The states of the lower and upper levels are denoted in jj coupling notation. All wavelengths are in nm. The calculated (λ_{calc}) and predicted (λ_{pred}) wavelengths are shown in the last two columns. References: *a* [45], *b* [46].

| λ_{LHD} | Ion | Lower Level | | Upper Level | | λ_{calc} | λ_{pred} |
		Conf.	State	Conf.	State		
5.829	Tm^{37+} [Ge]	3d^{10}4s^{2}4p^2	$(4p_-^2)_0$	3d^{10}4s^{2}4p4d	$(4p_-, 4d_-)_1$	5.804	—
5.911	Tm^{38+} [Ga]	3d^{10}4s^{2}4p	$4p_-$	3d^{10}4s^{2}4d	$4d_-$	5.891	—
6.003	Tm^{39+} [Zn]	3d^{10}4s4p	$(4s_+, 4p_-)_1$	3d^{10}4s4d	$(4s_+, 4d_-)_2$	5.999	—
6.072 †	Tm^{40+} [Cu]	3d^{10}4p	$4p_-$	3d^{10}4d	$4d_-$	6.069	6.0742 ^{a}
7.703	Tm^{38+} [Ga]	3d^{10}4s^{2}4p	$4p_-$	3d^{10}4s4p^2	$(4s_+, 4p_-, 4p_+)_{1/2}$	7.639	—
7.753	Tm^{39+} [Zn]	3d^{10}4s^2	$(4s_+^2)_0$	3d^{10}4s4p	$(4s_+, 4p_+)_1$	7.674	7.7442 ^{b}
7.832 *	Tm^{37+} [Ge]	3d^{10}4s^{2}4p^2	$(4p_-^2)_0$	3d^{10}4s4p^3	$(4s_+, 4p_+)_1$	7.786	—
7.832 *	Tm^{38+} [Ga]	3d^{10}4s^{2}4p	$4p_-$	3d^{10}4s4p^2	$(4s_+, 4p_-, 4p_+)_{3/2}$	7.796	—

* Blended. † Already reported in [25].

Table 2. The assignments of the lines of erbium ions indicated by arrows in the middle panel of Figure 1. The assignments are based on a comparison with the NIST EBIT data at a beam energy of 2.0 keV [29]. Isoelectronic sequence of each ion is shown in a square bracket. The states of the lower and upper levels are denoted in jj coupling notation. All wavelengths are in nm.

| λ_{LHD} | Ion | Lower Level | | Upper Level | | λ_{EBIT} |
		Conf.	State	Conf.	State	
6.099	Er^{36+} [Ge]	3d^{10}4s^{2}4p^2	$(4p_-^2)_0$	3d^{10}4s^{2}4p4d	$(4p_-, 4d_-)_1$	6.1041
6.171	Er^{37+} [Ga]	3d^{10}4s^{2}4p	$4p_-$	3d^{10}4s^{2}4d	$4d_-$	6.1755
6.271	Er^{38+} [Zn]	3d^{10}4s4p	$(4s_+, 4p_-)_1$	3d^{10}4s4d	$(4s_+, 4d_-)_2$	6.2733
6.334 †	Er^{39+} [Cu]	3d^{10}4p	$4p_-$	3d^{10}4d	$4d_-$	6.3391
8.080	Er^{37+} [Ga]	3d^{10}4s^{2}4p	$4p_-$	3d^{10}4s4p^2	$((4s_+, 4p_-)_1, 4p_+)_{1/2}$	8.0777

† Already reported in [25].

Table 3. The assignments of the lines of samarium ions indicated by arrows in the bottom panel of Figure 1. The assignments are based on a comparison with the NIST EBIT data at a beam energy of 1.25–2.20 keV [29]. Isoelectronic sequence of each ion is shown in a square bracket. The states of the lower and upper levels are denoted in jj coupling notation. All wavelengths are in nm.

| λ_{LHD}	Ion	Lower Level		Upper Level		λ_{EBIT}
		Conf.	State	Conf.	State	
6.857	Sm^{34+} [Ni]	$3d^9 4p$	$((3d^3_-)_{3/2}, 4p_-)_1$	$3d^9 4d$	$((3d^3_-)_{3/2}, 4d_-)_0$	6.8494
7.362	Sm^{34+} [Ni]	$3d^9 4p$	$((3d^5_+)_{5/2}, 4p_+)_1$	$3d^9 4d$	$((3d^3_-)_{3/2}, 4d_-)_0$	7.3563
7.750	Sm^{31+} [Ga]	$3d^{10} 4s^2 4p$	$4p_-$	$3d^{10} 4s^2 4d$	$4d_-$	7.7461
8.215 *	Sm^{31+} [Ga]	$3d^{10} 4s^2 4p$	$4p_-$	$3d^{10} 4s 4p^2$	$(4s_+, (4p^2_+)_2)_{3/2}$	8.2146
8.215 *†	Sm^{33+} [Cu]	$3d^{10} 4p$	$4p_-$	$3d^{10} 4d$	$4d_-$	8.2176
9.912	Sm^{32+} [Zn]	$3d^{10} 4s 4d$	$(4s_+, 4d_+)_2$	$3d^{10} 4s 4f$	$(4s_+, 4f_+)_3$	9.9127
10.087	Sm^{32+} [Zn]	$3d^{10} 4s 4p$	$(4s_+, 4p_+)_1$	$3d^{10} 4s 4d$	$(4s_+, 4d_+)_2$	10.0851
10.132	Sm^{31+} [Ga]	$3d^{10} 4s^2 4p$	$4p_+$	$3d^{10} 4s^2 4d$	$4d_-$	10.1294

* Blended. † Already reported in [25].

If available, comparisons with charge-resolved spectra taken in EBITs are powerful tools for interpreting the measured spectra. For Er and Sm, experimental data taken in the NIST EBIT have recently been reported [29]. Therefore, we have compared the high-temperature spectra of Er and Sm with the NIST EBIT data. The Er spectrum shown in the middle panel of Figure 1 is very similar to the NIST EBIT spectrum taken at the beam energy of 2 keV. Because the electron beam at the EBIT is almost mono-energetic, this similarity implies that the LHD spectrum is composed of only a few ion stages accumulated inside the plasma core region. The assignments of the prominent lines indicated by arrows are listed in Table 2, which shows the spectral feature is dominantly composed of only a few ion stages from Cu- to Ge-like ions. A similar comparison has been performed for the Sm spectrum shown in the bottom panel of Figure 1, and the resulting assignments are shown in Table 3. In this case, the LHD spectrum can be well explained by a combination of the EBIT spectra for several different beam energies in the range of 1.25–2.20 keV, including lines of Ni- to Ga-like ions. This is probably because the LHD spectrum in this case is composed of the integrated emission spread in wider region in the plasma.

5. Analysis of Low-Temperature Spectra

In general, it would be more difficult to construct CR models for the quasicontinuum UTA features to correctly reproduce the measured spectra in low-temperature conditions. Nevertheless, comparisons with theoretical calculations of line strength (gA values) distributions are possible for further assignments of the measured spectral peaks. For example, Figure 2 shows a soft X-ray spectrum of Tm ions recorded in an LHD plasma under a low-temperature condition, as well as the line strength distribution of 4d–4f transitions of Tm^{22+}–Tm^{24+} ions calculated by the Cowan code. The peak electron temperature for the LHD spectrum is approximately 0.7 keV. A narrowed UTA feature, the center wavelength of which is around 5.7 nm, with a bandwidth of approximately 0.3 nm is observed with several peaks superposed as indicated by arrows in the top panel of Figure 2. As a result of the comparison, most of the peaks have been assigned to the lines of Tm^{22+}–Tm^{24+} ions as listed in Table 4. The wavelengths of most of these lines are predicted by an interpolation of Z dependence in earlier studies [47–49], some of which have been recently identified in an LPP [15]. These predicted and measured wavelengths in the earlier studies are also listed in Table 4, and are in very good agreement with the present measurement. This result also indicates that the major peaks of the narrowed UTA feature in the low-temperature spectra can be well explained only by a few ion stages with simple electron configurations such as Ag-, Pd-, and Rh-like ions. As the similar UTA features with several peaks superposed are observed for most lanthanide elements under low-temperature conditions,

similar analyses for the other elements will lead to further assignments of the spectral lines of these ion stages.
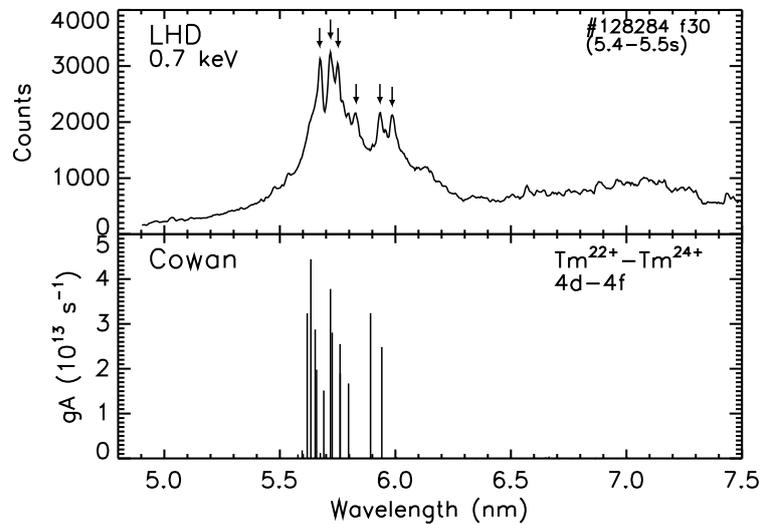
Figure 2. Soft X-ray spectrum of thulium ions recorded in an LHD plasma under a low-temperature condition (top panel) and the line strength (gA values) distribution of 4d–4f transitions of Tm^{22+}–Tm^{24+} ions calculated by Cowan code (bottom panel). The peak electron temperature for the LHD spectrum is approximately 0.7 keV. The assignments of the spectral lines indicated by arrows are summarized in Table 4.

Table 4. The assignments of the lines of thulium ions indicated by arrows in the top panel of Figure 2. The assignments are based on a comparison with the Cowan code calculation. Isoelectronic sequence of each ion is shown in a square bracket. The states of the lower and upper levels are denoted in LS coupling notation. All wavelengths are in nm. The wavelengths measured in the LPP (λ_{LPP}) [15] and the wavelengths predicted in the earlier studies (λ_{pred}) are listed in the last two columns. References: *a* [47], *b* [48], *c* [49].

λ_{LHD}	Ion	Lower Level		Upper Level		λ_{calc}	λ_{LPP}	λ_{pred}
		Conf.	State	Conf.	State			
5.672 [†]	Tm^{23+} [Pd]	$4d^{10}$	$^1S_0$	$4d^9 4f$	$^1P_1$	5.690	5.676 *	5.6754 [a]
5.719 *	Tm^{22+} [Ag]	$4d^{10} 4f$	$^2F_{7/2}$	$4d^9 4f^2$	$^2D_{5/2}$	5.653	—	5.7181 [b]
5.719 *	Tm^{22+} [Ag]	$4d^{10} 4f$	$^2F_{5/2}$	$4d^9 4f^2$	$^2D_{3/2}$	5.659	—	5.7178 [b]
5.752 *	Tm^{24+} [Rh]	$4d^9$	$^2D_{5/2}$	$4d^8 4f$	$^2F_{7/2}$	5.719	5.754 *	5.7504 [c]
5.752 *	Tm^{24+} [Rh]	$4d^9$	$^2D_{3/2}$	$4d^8 4f$	$^2F_{5/2}$	5.727	5.754 *	5.7562 [c]
5.830	Tm^{24+} [Rh]	$4d^9$	$^2D_{3/2}$	$4d^8 4f$	$^2D_{3/2}$	5.797	—	—
5.933 [†]	Tm^{22+} [Ag]	$4d^{10} 4f$	$^2F_{7/2}$	$4d^9 4f^2$	$^2G_{9/2}$	5.893	5.937 [‡]	5.9359 [b]
5.986 [†]	Tm^{22+} [Ag]	$4d^{10} 4f$	$^2F_{5/2}$	$4d^9 4f^2$	$^2G_{7/2}$	5.941	5.988	5.9865 [b]

* Blended. [†] Already reported in [25]. [‡] Tentative identification.

6. Summary

Soft X-ray spectra from several high Z rare-earth ions have been systematically observed in LHD plasmas, in which spectra from N shell ions appear as discrete or quasicontinuum UTA features depending on the electron temperature. The measured spectra are currently being analyzed by several different atomic codes and comparisons with existing experimental data. The discrete spectra observed in high-temperature conditions seem to be well reproduced by a CR model constructed based on the Hullac code, which can lead to the identifications of the spectral lines of higher charge states from Cu- to Ge-like ions. Also, it has been demonstrated that charge-resolved data of EBITs are powerful for the interpretation of the spectra. Although the detailed interpretation of the UTA feature

in low-temperature conditions would be more difficult, a comparison with Cowan code calculation has shown that the narrowed UTA feature can be well explained only by a few ion stages around Pd-like ions. By exploiting these tools, further analyses of most of the lanthanide elements are expected in the near future.

Author Contributions: Conceptualization, C.S., F.K. and I.M.; formal analysis, C.S., F.K., I.M. and G.O.; methodology, C.S., N.T. and S.S.; software, F.K., I.M. and G.O.; resources, C.S., N.T. and S.S.; investigation, C.S., F.K., I.M., N.T. and G.O.; writing—original draft preparation, C.S.; project administration, C.S.; funding acquisition, C.S. and N.T.

Conflicts of Interest: The authors declare no conflict of interest.

References

1. Bauche, J.; Bauche-Arnoult, C.; Klapisch, M.; Mandelbaum, P.; Schwob, J.-L. Quenching of transition arrays through configuration mixing. *J. Phys. B At. Mol. Opt. Phys.* **1987**, *20*, 1443–1450. [CrossRef]
2. Kilbane, D.; Cummings, A.; McGuinness, C.; Murphy, N.; O'Sullivan, G. 4f collapse, level density inflation and the emergence of 'compound-like' atomic states in rare earth ions. *J. Phys. B At. Mol. Opt. Phys.* **2002**, *35*, 309–321. [CrossRef]
3. Tong, X.-M.; Kato, D.; Watanabe, T.; Ohtani, S. Mechanisms of giant resonance in 4d photoionization of Eu. *J. Phys. B At. Mol. Opt. Phys.* **2000**, *33*, 717–725. [CrossRef]
4. Churilov, S.S.; Kildiyarova, R.R.; Ryabtsev, A.N.; Sadovsky, S.V. EUV spectra of Gd and Tb ions excited in laser-produced and vacuum spark plasmas. *Phys. Scr.* **2009**, *80*, 045303. [CrossRef]
5. Otsuka, T.; Kilbane, D.; White, J.; Higashiguchi, T.; Yugami, N.; Yatagai, T.; Jiang, W.; Endo, A.; Dunne, P.; O'Sullivan, G. Rare-earth plasma extreme ultraviolet sources at 6.5–6.7 nm. *Appl. Phys. Lett.* **2010**, *97*, 111503. [CrossRef]
6. Higashiguchi, T.; Otsuka, T.; Yugami, N.; Jiang, W.; Endo, A.; Li, B.; Kilbane, D.; Dunne, P.; O'Sullivan, G. Extreme ultraviolet source at 6.7 nm based on a low-density plasma. *Appl. Phys. Lett.* **2011**, *99*, 191502. [CrossRef]
7. Li, B.; Otsuka, T.; Higashiguchi, T.; Yugami, N.; Jiang, W.; Endo, A.; Dunne, P.; O'Sullivan, G. Investigation of Gd and Tb plasmas for beyond extreme ultraviolet lithography based on multilayer mirror performance. *Appl. Phys. Lett.* **2012**, *101*, 013112. [CrossRef]
8. O'Sullivan, G.; Li, B.; Dunne, P.; Hayden, P.; Kilbane, D.; Lokasani, R.; Long, E.; Ohashi, H.; O'Reilly, F.; Sheil, J.; et al. Sources for beyond extreme ultraviolet lithography and water window imaging. *Phys. Scr.* **2015**, *90*, 054002. [CrossRef]
9. O'Sullivan, G.; Li, B.; D'Arcy, R.; Dunne, P.; Hayden, P.; Kilbane, D.; McCormack, T.; Ohashi, H.; O'Reilly, F.; Sheridan, P.; et al. Spectroscopy of highly charged ions and its relevance to EUV and soft X-ray source development. *J. Phys. B At. Mol. Opt. Phys.* **2015**, *48*, 144025.
10. Sugar, J. Resonance lines in the Ag I and Pd I isoelectronic sequences: Cs IX through Sm XVI and Cs X through Nd XV. *J. Opt. Soc. Am.* **1977**, *67*, 1518–1521. [CrossRef]
11. Reader, J.; Luther, G. The copper isoelectronic sequence: Ba^{27+}–W^{45+}. *Phys. Scr.* **1981**, *24*, 732–737. [CrossRef]
12. O'Sullivan, G.; Carroll, P.K. 4d-4f emission resonances in laser-produced plasmas. *J. Opt. Soc. Am.* **1981**, *71*, 227–230. [CrossRef]
13. Carroll, P.K.; O'Sullivan, G. Ground-state configurations of ionic species I through XVI for Z = 57–74 and the interpretation of 4d-4f emission resonances in laser-produced plasmas. *Phys. Rev. A* **1982**, *25*, 275–286. [CrossRef]
14. Zeng, G.M.; Daido, H.; Nishikawa, T.; Takabe, H.; Nakayama, S.; Aritome, H.; Murai, K.; Kato, Y.; Nakatsuka, M.; Nakai, S. Soft X-ray spectra of highly ionized elements with atomic numbers ranging from 57 to 82 produced by compact lasers. *J. Appl. Phys.* **1994**, *75*, 1923–1930. [CrossRef]
15. Sheil, J.; Dunne, P.; Higashiguchi, T.; Kos, D.; Long, E.; Miyazaki, T.; O'Reilly, F.; O'Sullivan, G.; Sheridan, P.; Suzuki, C.; et al. Analysis of soft X-ray emission spectra of laser-produced dysprosium, erbium and thulium plasmas. *J. Phys. B At. Mol. Opt. Phys.* **2017**, *50*, 065006. [CrossRef]

16. Lokasani, R.; Sheil, J.; Barte, E.F.; Hara, H.; Tamura, T.; Gisuji, T.; Higashiguchi, T.; Suzuki, C.; Dunne, P.; O'Sullivan, G.; et al. Soft X-ray spectral analysis of samarium plasmas produced by solid-state laser pulses. *J. Phys. B At. Mol. Opt. Phys.* **2018**, *51*, 215001. [CrossRef]

17. Finkenthal, M.; Lippmann, A.S.; Huang, L.K.; Yu, T.L.; Stratton, B.C.; Moos, H.W.; Klapisch, M.; Mandelbaum, P.; Bar Shalom, A.; Hodge, W.L.; et al. The spectrum of highly ionized praseodymium and dysprosium from the Texas tokamak plasma in the 50–250-Å range. *J. Appl. Phys.* **1986**, *59*, 3644–3649. [CrossRef]

18. Mandelbaum, P.; Finkenthal, M.; Schwob, J.L.; Klapisch, M. Interpretation of the quasicontinuum band emitted by highly ionized rare-earth elements in the 70–100-Å range. *Phys. Rev. A* **1987**, *35*, 5051–5059. [CrossRef]

19. Finkenthal, M.; Moos, H.W.; Bar-Shalom, A.; Spector, N.; Zigler, A.; Yarkoni, E. Electron-density dependence of line intensities of Cu I-like Sm^{33+} to Yb^{41+} emitted from tokamak and laser-produced plasmas. *Phys. Rev. A* **1988**, *38*, 288–295. [CrossRef]

20. Finkenthal, M.; Lippmann, S.; Huang, L.K.; Moos, H.W.; Lee, Y.T.; Spector, N.; Zigler, A.; Yarkoni, E. $\Delta n = 0$ *N*-shell emission of rare-earth ions ($Z = 59$ to 70) emitted from low and high-density tokamak and laser-produced plasmas. *Phys. Scr.* **1990**, *41*, 445–448. [CrossRef]

21. Mandelbaum, P.; Finkenthal, M.; Meroz, E.; Schwob, J.L.; Oreg, J.; Goldstein, W.H.; Osterheld, L.; Bar-Shalom, A.; Lippmann, S.; Huang, L.K.; et al. Effect of excitation-autoionization processes on the line emission of Zn I- and Ga I-like rare-earth ions in hot coronal plasmas. *Phys. Rev. A* **1990**, *42*, 4412–4415. [CrossRef] [PubMed]

22. Fournier, K.B.; Goldstein, W.H.; Osterheld, A.; Finkenthal, M.; Lippmann, S.; Huang, L.K.; Moos, H.W.; Spector, N. Soft X-ray emission of galliumlike rare-earth atoms produced by high-temperature low-density tokamak and high-density laser plasmas. *Phys. Rev. A* **1994**, *50*, 2248–2256. [CrossRef] [PubMed]

23. Suzuki, C.; Koike, F.; Murakami, I.; Tamura, N.; Sudo, S. Observation of EUV spectra from gadolinium and neodymium ions in the Large Helical Device. *J. Phys. B At. Mol. Opt. Phys.* **2012**, *45*, 135002. [CrossRef]

24. Suzuki, C.; Koike, F.; Murakami, I.; Tamura, N.; Sudo, S. Temperature dependent EUV spectra of Gd, Tb and Dy ions observed in the Large Helical Device. *J. Phys. B At. Mol. Opt. Phys.* **2015**, *48*, 144012. [CrossRef]

25. Suzuki, C.; Koike, F.; Murakami, I.; Tamura, N.; Sudo, S. Systematic observation of EUV spectra from highly charged lanthanide ions in the Large Helical Device. *Atoms* **2018**, *6*, 24. [CrossRef]

26. Kilbane, D.; O'Sullivan, G.; Gillaspy, J.D.; Ralchenko, Y.; Reader, J. EUV spectra of Rb-like to Cu-like gadolinium ions in an electron-beam ion trap. *Phys. Rev. A* **2012**, *86*, 042503. [CrossRef]

27. Ohashi, H.; Sakaue, H.A.; Nakamura, N. Extreme ultra-violet emission spectroscopy of highly charged gadolinium ions with an electron beam ion trap. *Phys. Scr.* **2013**, *T156*, 014013. [CrossRef]

28. Kilbane, D.; O'Sullivan, G.; Podpaly, Y.A.; Gillaspy, J.D.; Reader, J.; Ralchenko, Y. EUV spectra of Rb-like to Ni-like dysprosium ions in an electron beam ion trap. *Eur. Phys. J. D* **2014**, *68*, 222. [CrossRef]

29. Podpaly, Y.A.; Gillaspy, J.D.; Reader, J.; Ralchenko, Y. Measurements and identifications of extreme ultraviolet spectra of highly-charged Sm and Er. *J. Phys. B At. Mol. Opt. Phys.* **2015**, *48*, 025002. [CrossRef]

30. Takeiri, Y.; Morisaki, T.; Osakabe, M.; Yokoyama, M.; Sakakibara, S.; Takahashi, H.; Nakamura, Y.; Oishi, T.; Motojima, G.; Murakami, S.; et al. Extension of the operational regime of the LHD towards a deuterium experiment. *Nucl. Fusion* **2017**, *57*, 102023. [CrossRef]

31. Takeiri, Y. Advanced Helical Plasma Research towards a Steady-State Fusion Reactor by Deuterium Experiments in Large Helical Device. *Atoms* **2018**, *6*, 69. [CrossRef]

32. Sudo, S.; Tamura, N.; Khlopenkov, K.; Muto, S.; Funaba, H.; Viniar, I.; Sergeev, V.; Sato, K.; Ida, K.; Kawahata, K.; et al. Particle transport diagnostics on CHS and LHD with tracer-encapsulated solid pellet injection. *Plasma Phys. Control. Fusion* **2002**, *44*, 129–135. [CrossRef]

33. Sudo, S.; Tamura, N. Tracer-encapsulated solid pellet injection system. *Rev. Sci. Instrum.* **2012**, *83*, 023503. [CrossRef] [PubMed]

34. Narihara, K.; Yamada, I.; Hayashi, H.; Yamauchi, K. Design and performance of the Thomson scattering diagnostic on LHD. *Rev. Sci. Instrum.* **2001**, *72*, 1122–1125. [CrossRef]

35. Yamada, I.; Narihara, K.; Funaba, H.; Hayashi, H.; Kohmoto, T.; Takahashi, H.; Shimozuma, T.; Kubo, S.; Yoshimura, Y.; Igami, H.; et al. Improvements of data quality of the LHD Thomson scattering diagnostics in high-temperature plasma experiments. *Rev. Sci. Instrum.* **2010**, *81*, 10D522. [CrossRef] [PubMed]

36. Schwob, J.L.; Wouters, A.W.; Suckewer, S.; Finkenthal, M. High-resolution duo-multichannel soft-X-ray spectrometer for tokamak plasma diagnostics. *Rev. Sci. Instrum.* **1987**, *58*, 1601–1615. [CrossRef]

37. Suzuki, C.; Koike, F.; Murakami, I.; Tamura, N.; Sudo, S.; Sakaue, H.A.; Nakamura, N.; Morita, S.; Goto, M.; Kato, D.; et al. EUV spectroscopy of highly charged high Z ions in the Large Helical Device plasmas. *Phys. Scr.* **2014**, *89* 114009. [CrossRef]
38. Suzuki, C.; Murakami, I.; Koike, F.; Tamura, N.; Sakaue, H.A.; Morita, S.; Goto, M.; Kato, D.; Ohashi, H.; Higashiguchi, T.; et al. Extreme ultraviolet spectroscopy and atomic models of highly charged heavy ions in the Large Helical Device. *Plasma Phys. Control. Fusion* **2017**, *59*, 014009. [CrossRef]
39. Bauche, J.; Bauche-Arnoult, C.; Klapisch, M. Unresolved transition arrays. *Phys. Scr.* **1988**, *37*, 659–663. [CrossRef]
40. Parpia, F.A.; Fischer, C.F.; Grant, I.P. GRASP92: A package for large-scale relativistic atomic structure calculations. *Comput. Phys. Commun.* **2006**, *175*, 745–747. [CrossRef]
41. Fritzsche, S. The RATIP program for relativistic calculations of atomic transition, ionization and recombination properties. *Comput. Phys. Commun.* **2012**, *183*, 1525–1559. [CrossRef]
42. Cowan, R.D. *The Theory of Atomic Structure and Spectra*; University of California Press: Berkeley, CA, USA, 1991.
43. Bar-Shalom, A.; Klapisch, M.; Oreg, J. HULLAC, an integrated computer package for atomic processes in plasmas. *J. Quant. Spectrosc. Radiat. Transf.* **2001**, *71*, 169–188. [CrossRef]
44. Gu, M.F. The flexible atomic code. *Can. J. Phys.* **2008**, *86*, 675–689. [CrossRef]
45. Seely, J.F.; Brown, C.M.; Feldman, U. Wavelengths and energy levels for the Cu I isoelectronic sequence Ru^{15+} through U^{63+}. *At. Data Nucl. Data Tables* **1989**, *43*, 145–159. [CrossRef]
46. Brown, C.M.; Seely, J.F.; Kania, D.R.; Hammel, B.A.; Back, C.A.; Lee, R.W.; Bar-Shalom, A.; Behring, W.E. Wavelengths and energy levels for the Zn I isoelectronic sequence Sn^{20+} through U^{62+}. *At. Data Nucl. Data Tables* **1994**, *58*, 203–217. [CrossRef]
47. Sugar, J.; Kaufman, V.; Rowan, W.L. Observation of Pd-like resonance lines through Pt^{32+} and Zn-like resonance lines of Er^{38+} and Hf^{42+}. *J. Opt. Soc. Am. B* **1993**, *10*, 799–801. [CrossRef]
48. Sugar, J.; Kaufman, V.; Rowan, W.L. Spectra of Ag I isoelectronic sequence observed from Er^{21+} to Au^{32+}. *J. Opt. Soc. Am. B* **1993**, *10*, 1321–1325. [CrossRef]
49. Sugar, J.; Kaufman, V.; Rowan, W.L. Rh I isoelectronic sequence observed from Er^{23+} to Pt^{33+}. *J. Opt. Soc. Am. B* **1993**, *10*, 1977–1979. [CrossRef]